Journal of Nanoparticle Research **6:** 301–305, 2004.

Brief communication

Physical characteristics and sintering behavior of MgO-doped ZrO_2 nanoparticles

E.N.S. Muccillo, S.K. Tadokoro and R. Muccillo
Centro Multidisciplinar para o Desenvolvimento de Materiais Cerâmicos, Instituto de Pesquisas Energéticas e Nucleares–CCTM, C.P. 11049, Pinheiros 05422-970, S. Paulo, SP, Brazil (Tel.: 55-11-38169343; Fax: 55 11 38169370; E-mail: enavarro@usp.br)

Received 21 October 2003; accepted in revised form 11 April 2004

Key words: zirconia, nanoparticles, TEM, pore size distribution, sintering

Abstract

Nanosized particles of 13 mol% MgO-doped ZrO_2 with a narrow distribution of pore sizes were prepared by the coprecipitation technique using optimized parameters of synthesis. Transmission electron microscopy analysis of the calcined powder reveals that the majority of the particles have grain sizes in the 10–20 nm range. From nitrogen adsorption analysis an average particle size of 13 nm was estimated, which is similar to the average pore size diameter (12 nm). Besides the unimodal distribution of pore sizes, the linear shrinkage curve of a powder compact exhibits several inflexions indicating different rates of densification up to 1600°C. After sintering at 1600°C for 2 h, the microstructure features of a compact are characteristics of the intermediate stage with interconnected porosity preferentially observed at grain boundaries. These results are explained as a size effect of nanoparticles of magnesia-doped zirconia during sintering.

Introduction

Zirconia-based ceramics are very important materials for a number of high-technology applications (Subbarao, 1981). They may be used not only as a structural ceramic but also as a functional material. Magnesium-doped zirconia solid solution is a solid electrolyte known for its use to monitor the oxygen content in molten steel (Janke, 1981). The MgO content in this case, is 7–8.5 mol%, and this material has been thoroughly studied with respect to its electrical and mechanical properties. In contrast, few studies have been carried out on magnesium fully stabilized zirconia (Mg-FSZ). Experimental studies on Mg-FSZ have focused on the diffusional behavior of oxygen and cations (Sakka et al., 1982; Ando et al., 1985), the ionic conductivity and mechanical properties (Muccillo & Kleitz, 1995; Ábrahám & Gritzner, 1996), and the occurrence of a tetragonal t′-phase and its microstructural development (Caracoche et al., 1993). Recently, Mg-FSZ has been suggested as a candidate for preparing a ceramic nanofiltration membrane. The nanosized zirconia powder containing 13 mol% MgO (Mg-FSZ) was prepared by the sol–gel technique using alkoxide precursors (Vacassy et al., 1998).

Interest in nanocrystalline zirconia ceramics has increased in the past few years as their properties are different and considerably improved compared with conventional ceramics. Nanophase processing powders can usually lead to a homogeneous microstructure, high densification and uniform grain size distribution in the sintered ceramic. Moreover, processing temperatures may be considerably lower than those used for conventional ceramic powders (Chen & Mayo, 1996; Betz et al., 2000). The main problem during processing of nanocrystalline ceramic materials is their instability at high temperatures. As a consequence of the

large excess free energy, significant grain growth has been observed in these materials (Mayo, 1996).

Currently, several production techniques are available for the synthesis of nanoparticles employing the three phases, namely the solid, the solution and the vapor phase (Siegel, 1993). Although the solution methods present some disadvantages related mainly to agglomeration and purity of the powder, their low-cost and relatively good reproducibility make them more attractive from the viewpoint of a possible industrial application. Thus, in spite of these disadvantages, the aqueous coprecipitation methods are the most widely used to prepare nanoscale ceramic powders (Segal, 1998).

In this paper, the preparation of 13 mol% MgO-doped ZrO_2 nanoparticles using an optimized coprecipitation method is reported. This work was also undertaken to verify the sintering behavior of these nanoparticles. The pore size distribution and the specific surface area were obtained by nitrogen adsorption experiments, and the morphology of nanoparticles was examined by transmission electron microscopy. The sintering behavior of powder compacts was studied by linear shrinkage and scanning electron microscopy.

Experimental procedure

Zirconyl chloride, $ZrOCl_2{\cdot}8H_2O$ (>98%, BDH) and magnesium nitrate, $Mg(NO_3)_2{\cdot}6H_2O$ (>99%, Vetec) were used as starting materials. Stock solutions of these salts were prepared with deionized water. Suitable amounts of these solutions were thoroughly mixed in the desired proportion, and the resulting solution was added under constant stirring to an ammonium chloride solution to effect the coprecipitation. During this step, the pH of precipitation was kept constant and above 9. The precipitate was digested in the mother liquid for 2 h after precipitation completion. Washing the precipitate was carried out with a diluted ammonia solution followed by two cycles of washing with isopropyl alcohol and vacuum filtration. Further dehydration was accomplished by azeotropic distillation of the gel with *n*-butyl alcohol. During coprecipitation experiments, a number of variables was controlled to ensure reproducibility. These variables were selected from previous works (Suzuki, 1986; Ávila & Muccillo, 1995; Muccillo & Ávila, 1999; Tadokoro & Muccillo, 2002a, b). Thermal decomposition of the gel was performed at 600°C for 1 h. The nominal MgO content in the solid solution was 13 mol%, which corresponds to a FSZ. Cylindrical specimens were prepared by uniaxial followed by isostatic pressing at 206 MPa.

Nitrogen adsorption/desorption (ASAP 2010, Micromeritics) experiments were carried out to determine the specific surface area, *S*, by the Brunauer, Emmett and Teller (BET) method, and the distribution of pore sizes by the Barret, Joyner and Halenda (BJH) method. The morphology of powder particles was examined using transmission electron microscopy (CM200, Philips). Linear shrinkage (DIL 402 E/7, Netzsch) in a powder compact was followed up to 1650°C with a heating rate of $10°C{\cdot}min^{-1}$. The microstructure of sintered pellets was observed on fractured surfaces by scanning electron microscopy, SEM (XL30, Philips) using secondary electrons.

Results and discussion

Figure 1 shows a TEM micrograph of calcined Mg-FSZ nanoparticles. These nanoparticles are uniform in size and shape, and weakly agglomerated into spherical clusters. The distribution of particle sizes is relatively narrow as most of them have a diameter between 10 and 20 nm.

The specific surface area determined by the BET method is 77 $m^2{\cdot}g^{-1}$. Assuming a theoretical density of 5.9 $g{\cdot}cm^{-3}$ for the studied composition, an equivalent particle size of 13 nm was estimated

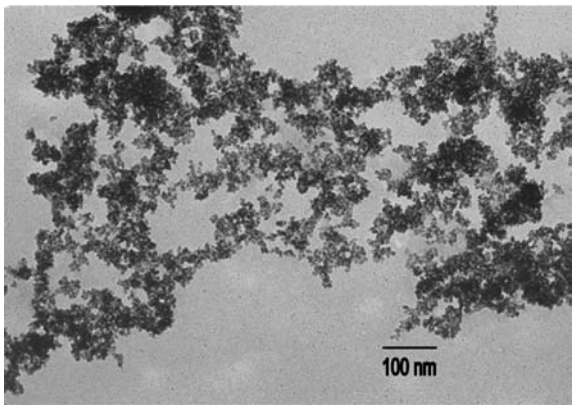

Figure 1. TEM micrograph of calcined Mg-FSZ nanoparticles.

from the BET analysis. This result is in good agreement with that of TEM.

A typical adsorption/desorption isotherm is shown in Figure 2. This isotherm is of type IV according to BDDT classification (Sing et al., 1985), and characteristic of a well-developed system containing mesopores. The hysteresis loop is characterized by adsorption and desorption branches nearly parallel to each other in a considerable range of P/P_0. This type of loop is frequently obtained for approximately spherical agglomerated particles with uniform size and coordination number.

Figure 3 shows the pore size distribution curve obtained by the BJH method, assuming a cylindrical pore model. A unimodal distribution of pore sizes with an average size of 12 nm may be seen in this figure. Conventional doped-zirconia powders usually present a bimodal distribution of pore sizes assigned to intra- and interagglomerate pores. The latter are removed later during sintering, taking part in the densification process, and influencing grain growth rates (Halloran, 1984). The present result is attributed to the use of optimized parameters during the synthesis of nanoparticles.

These results based on adsorption measurements demonstrate the possibility of using this solid solution for applications such as heterogeneous catalysis and electrocatalysis, which require materials with high specific surface area and mesoporous structure (Trudeau & Ying, 1996).

The adsorption/desorption isotherm of ceria-doped zirconia (Tadokoro & Muccillo, 2002b) synthesized by the same technique has a similar

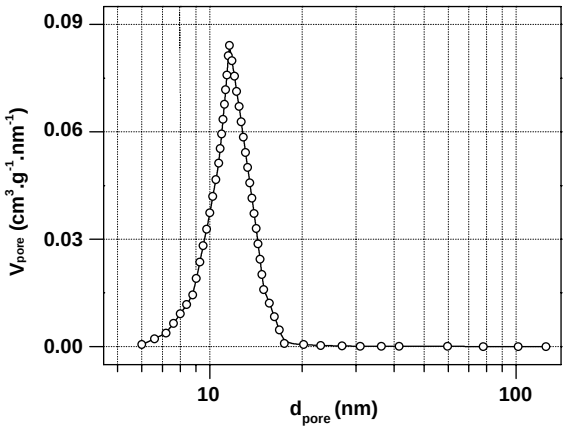

Figure 3. Pore size distribution of Mg-FSZ nanoparticles obtained by the BJH method.

shape as that of Figure 2. However, the specific surface area was higher ($\sim$128 $m^2\ g^{-1}$), and the average pore size was lower ($\sim$9 nm). This shows that the structure of these solid solutions is determined by the type and concentration of the dopant cation.

The linear shrinkage of a powder compact and its derivative curve are shown in Figure 4. The total shrinkage is 23% and most of it occurs in the temperature range between 800°C and 1300°C. The maximum shrinkage rate occurs at 885°C, and above this temperature the densification process is slowed down. Other inflexions observed at higher temperatures may be assigned to crystallographic phase transformations (monoclinic-to-tetragonal and tetragonal-to-cubic), which are known to occur in zirconia-based ceramics (Subbarao, 1981).

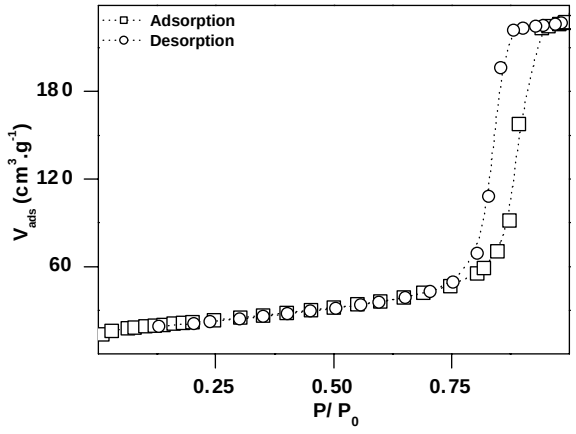

Figure 2. Adsorption/desorption isotherm of Mg-FSZ nanoparticles.

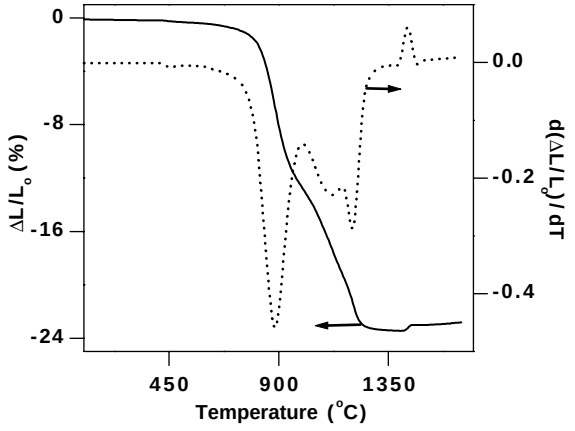

Figure 4. Linear shrinkage curve of a Mg-FSZ compact and its derivative curve.

On sintering a ceramic powder compact, densification and grain growth are expected to take place simultaneously to different extents, depending on intrinsic and extrinsic factors such as the sintering temperature and time, initial particle size, particle packing configuration, sintering atmosphere, dopants (content and type), and others. The curves in Figure 4 show clearly that the densification of the compact proceeds in several steps, and that the densification rate depends on the crystallographic phase.

Figure 5 shows a typical SEM micrograph of the fractured surface of a compact sintered at 1600°C for 2 h. The predominant fracture mode is transgranular. It is worth noting that the residual porosity is apparently found at the grain boundaries and triple junctions. In fact, this interconnected porosity delineates the grain boundaries, and shows that the sintering process did not reach the final sintering stage.

Conventional microcrystalline powders sintered at high temperatures and for longer times have an average grain size ≥20 μm with extensive closed porosity (Muccillo & Kleitz, 1995). These microstructure features are attributed to fast grain growth, and to the relatively low pore mobility, which are typical of FSZs. As shown in Figure 5, however, grain growth is not fast, in this case. A full discussion on the exact mechanism as to why this occur is outside the scope of this paper. However, a possible explanation for this effect is a change in the kinetics of grain growth due to the small size of particles. Recent investigations have established that the thermodynamic properties of nanocrystalline solids are particle-size dependent (Tolbert & Alivisatos, 1994). Moreover, MgO particles have very low solubility in zirconia (Grain, 1967). Thus, segregation of MgO particles may have occurred during sintering and could have produced a solute drag effect reducing the boundary mobility. Indeed, one of the usual approaches to control grain growth in ceramic materials is the use of specific additives (Brook, 1982). The important point stressed here is that SEM observation evidences the retardation of the sintering process. Therefore, the main mechanism of sintering Mg-FSZ prepared from nanoparticles is characterized by a low pore elimination kinetics along with reduced boundary mobility.

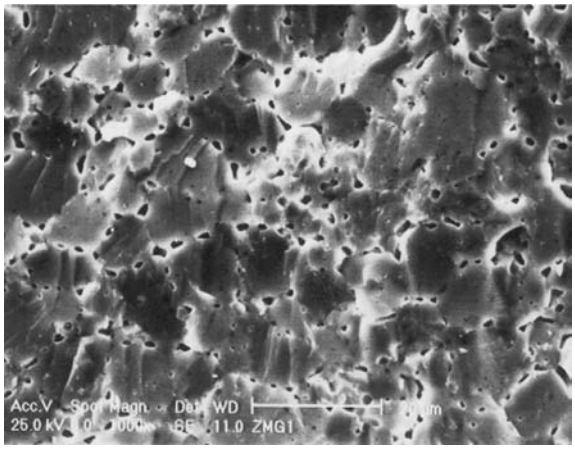

Figure 5. SEM micrograph of a fractured surface of a Mg-FSZ sintered compact.

Conclusions

Nanoparticles of ZrO_2-13 mol% MgO were prepared by an optimized coprecipitation process. These nanoparticles with an average size of 13 nm have a narrow and unimodal distribution of pore sizes. The linear shrinkage of the powder compacts are characterized by several steps of densification according to crystallographic phase transformations. Microstructure features of the sintered compacts evidence different kinetic effects of pore elimination and grain growth probably due to the small size of the particles.

Acknowledgements

To FAPESP (97/14238-4 and 95/00544-0), CNPq (300934/94-7), CNEN, and PRONEX. To prof. H.S. Santos of IFUSP for TEM observations, and to the Laboratory of Structural Ceramics at IPEN for the linear shrinkage measurement.

References

Ábrahám I. & G. Gritzner, 1996. J. Eur. Ceram. Soc. 16, 71.
Ando K., Y. Oishi, H. Koizumi & Y. Sakka, 1985. J. Mater. Sci. Lett. 4, 176.
Ávila, D.M. & E.N.S. Muccillo, 1995. Thermochim. Acta 256, 391.
Betz, U., A. Sturm, J.F. Löffler, W. Wagner, A. Wiedenmann & H. Hahn, 2000. Mater. Sci. Eng. A 281, 68.
Brook, R., 1982. Proc. Brit. Ceram. Soc. 32, 7.

Caracoche M.C., P.C. Rivas, A.F. Pasquevich, A.R. López-Garcia, E. Aglietti & A. Scian, 1993. J. Mater. Res. 8, 605.
Chen, D.-J. & M.J. Mayo, 1996. J. Am. Ceram. Soc. 79, 906.
Grain, C.F. 1967. J. Am. Ceram. Soc. 50, 288.
Halloran, J.H., 1984. Role of powder agglomerates in ceramic processing. In: Mangels J.A. and Messing, G.L. eds. Advances in Ceramics, Vol. 9, Forming of Ceramics, Am. Ceram. Soc., Columbus, Ohio, p. 67.
Janke, D., 1981. Zirconia, hafnia, and thoria-based electrolytes for oxygen control in metallurgical processes. In: Heuer A.H. and Hobbs L.W. eds. Advances in Ceramics, Vol. 3, Science and Technology of Zirconia, American Ceramic Society, Columbus, Ohio, p. 419.
Mayo, M.J., 1996. Mater. Sci. Forum 204–206, 389.
Muccillo, E.N.S. & D.M. Ávila, 1999. Ceram. Int. 25, 345.
Muccillo E.N.S. & M. Kleitz, 1995. J. Eur. Ceram. Soc. 15, 51.
Sakka Y, Y. Oishi & K. Ando, 1982. Bull. Chem. Soc. Jpn. 55, 420.
Segal, D., 1998. Key Eng. Mater. 153–154, 241.
Siegel, R.W., 1993. Mater. Sci. Eng. A 168, 189.
Sing, K.S., D.H. Everett, R.A.W. Haul, L. Moscou, R.A. Pierotti, J. Rouquerol & T. Siemienivska, 1985. Pure Appl. Chem. 57, 603.
Subbarao, E.C., 1981. Zirconia-an overview. In: Heuer A.H. and Hobbs L.W. eds. Advances in Ceramics, Vol. 3, Science and Technology of Zirconia, American Ceramic Society, Columbus, Ohio, p. 1.
Suzuki, T., S. Osaka & N. Aikawa, 1986. Applied European Patent 0171736A2.
Tadokoro, S.K. & E.N.S. Muccillo, 2002a. J. Alloy Compd. 344, 186.
Tadokoro, S. K. & E.N.S. Muccillo, 2002b. J. Eur. Ceram. Soc. 22, 1723.
Tolbert, S.H. & A.P. Alivisatos, 1994. Science 265, 373.
Trudeau, M.L. & J.Y. Ying, 1996. Nanostruct. Mater. 7, 245.
Vacassy R., C. Guizard, J. Palmeri & L. Cot, 1998. Nanostruct. Mater. 10, 77.